Dun Chen, Tunsagnl Awut, Bin Liu, Yali Ma, Tao Wang and Ismayil Nurulla*

Functionalized magnetic Fe_3O_4 nanoparticles for removal of heavy metal ions from aqueous solutions

DOI 10.1515/epoly-2016-0043
Received February 18, 2016; accepted April 28, 2016; previously published online June 7, 2016

Abstract: Fe_3O_4 nanoparticles (MNP) were coated with 3-aminopropyltriethoxy-silane (APTES), resulting in anchoring of primary amine groups on the surface of the particles, then four kinds of novel magnetic adsorbents (Fe_3O_4@SiO_2-NH-HCGs) were formed by grafting of different heterocyclic groups (HCG) on amino groups via substitution reaction. These Fe_3O_4@SiO_2-NH-HCGs were characterized by scanning electron microscopy (SEM), transmission electron microscopy (TEM), Fourier transform infrared spectroscopy (FT-IR), X-ray diffraction (XRD) and energy disperse spectroscopy (EDS). The results confirmed the formation of Fe_3O_4@SiO_2-NH-HCGs nanoparticles and the Fe_3O_4 core possessed superparamagnetism. Batch experiments were performed to evaluate adsorption conditions of Cu^{2+}, Hg^{2+}, Pb^{2+} and Cd^{2+}. Under normal temperature and neutral condition, just 20 min, the removal efficiency of any Fe_3O_4@SiO_2-NH-HCGs is more than 96%. In addition, these Fe_3O_4@SiO_2-NH-HCGs have good stability and reusability. Their removal efficiency has no obvious decrease after being used seven times. After the experiments were finished, Fe_3O_4@SiO_2-NH-HCGs were conveniently separated via an external magnetic field due to superparamagnetism. These results indicate that these Fe_3O_4@SiO_2-NH-HCGs are potentially attractive materials for the removal of heavy metal ions from industrial wastewater.

***Corresponding author: Ismayil Nurulla,** Key Laboratory of Oil and Gas Fine Chemicals, Educational Ministry of China, School of Chemistry and Chemical Engineering, Xinjiang University, 14 Shengli road, Urumqi, Xinjiang 830046, P.R. China,
Phone: +86 0991 8583575, Fax: +86 0991 8583575,
e-mail: ismayilnu@sohu.com
Dun Chen and Yali Ma: Key Laboratory of Oil and Gas Fine Chemicals, Educational Ministry of China, School of Chemistry and Chemical Engineering, Xinjiang University, Urumqi 830046, P.R. China; and Xinjiang Education Institute, Urumqi 830043, P.R. China
Tunsagnl Awut: Key Laboratory of Oil and Gas Fine Chemicals, Educational Ministry of China, School of Chemistry and Chemical Engineering, Xinjiang University, Urumqi 830046, P.R. China
Bin Liu: Xinjiang Education Institute, Urumqi 830043, P.R. China
Tao Wang: Institute of Applied Chemistry, Xinjiang University, Urumqi 830046, P.R. China

Keywords: adsorbent; Fe_3O_4 nanoparticles; heavy metal ions removal; magnetic separation; removal efficiency.

1 Introduction

With the development of the world economy, environmental pollution has been a difficult problem that every country cannot avoid. Especially in rapid developing country, pollution problems frequently appear in news. For instances, rivers or land are polluted by wastewater from many industries such as battery manufacturing industries, tanneries, chemical manufacturing, mining, etc., containing a large number of heavy metal ions (1). Among these heavy metal ions, copper ions emission is the most common due to the wide use of copper, mercury ions and lead ions emission are a concern because of the high toxicity, everyone knows the harm of cadmium ion because of itai-itai disease. They are the most common toxic metal ions, listed in the 11 hazardous priority substances of pollutants, that can accumulate in living organisms, causing several disorders and diseases (2–4). How to remove the above heavy metal ions has become a hot topic for environmentalists and chemists. Numerous methods have been used including chemical precipitation, ion exchange, electrolysis, reverse osmosis processes, liquid-liquid extraction, resins, cementation (5–7). All of them have some disadvantages such as low efficiency, complexity, and high cost as well as secondary waste (8–10). Lately, the application of nanoadsorbence has attracted everyone's attention due to their excellent properties, such as high surface area, good adsorption property. However, the small particle size of a nanoparticle brings the difficulty of separating it from solutions, which limits the application in water treatment (11).

Fe_3O_4 nanoparticles (MNP) are a kind of new nanomaterials that exhibits properties such as being easy to recycle, magnetic separation, enrichment, chemical stability, biocompatibility, lower toxicity and price, superparamagnetism, uniform particle size distribution, high saturation magnetization, and a large surface area (12–18). They have been widely used in wastewater treatment,

cell separation, magnetic resonance imaging (MRI), drug delivery systems, and protein separation (19–22). Based on these excellent properties, Fe_3O_4 adsorbents emergence has been timely. Fe_3O_4 adsorbents are usually prepared by the functionalization of magnetic particles via direct silylation with silane coupling agents, organic vapor condensation, polymer coating and surfactant adsorption (23–25). When there is the presence of an external magnetic field, these superparamagnetic adsorbents are attracted to separate easily from the matrix. This overcomes the disadvantages of nanoadsorbents not being easy to separate from solution. Additionally, MNP were coated with silica shells, which bring chemical robustness and new chances of surface modification with a variety of chemical groups. For example, Zhang's group demonstrated thiol modified Fe_3O_4@SiO_2 as a robust, high effective and recycling magnetic sorbent for mercury removal (26).

Wang et al. (27) reported that Fe_3O_4 microspheres modified with the rhodamine hydrazide (Fe_3O_4-R6G) can be developed for selective detection and removal of mercury ion from water and the research results of Wang et al. (28) showed that magnetic mesoporous silica nanocomposites (MMS) can be used for the detection and removal of mercury ion, the composites both use the coordination of mercury ion and nitrogen atom to remove mercury. However, the proportion of donor atoms is low and the coordination efficiency of donor atoms is affected by steric hindrance in grafting groups. So, these defects reduce the adsorption capacity of composites. Mahdavian et al. (29) prepared Fe_3O_4 microspheres modified subsequently with 3-aminopropyl triethoxysilane, acryloyl chloride and acrylic acid, and found that the composites can be developed for removal of heavy metal ions. However, the synthesis method is complicated, which is not conducive to practical application.

In this work, (i) the synthesis of MNP and (ii) amine modified silica coated magnetite (Fe_3O_4@SiO_2-NH_2) were prepared by coating APTES on surface of MNP, (iii) four kinds of novel Fe_3O_4@SiO_2-NH-HCGs [HCG=py (2-pyridinyl); pyd (3-pyridazinyl); pya (2-pyrazinyl); pym (4-pyrimidinyl)] were formed by grafting of different heterocyclic groups on amino groups via substitution reaction. On the one hand, the grafting method is simple and magnetic Fe_3O_4@SiO_2-NH-HCGs can be easily separated from solution by an external magnetic field. On the other hand, the nitrogen atoms of HCGs, which possesses a high proportion, strong coordination ability and low steric hindrance, can drastically improve the adsorption of the heavy metals. Fe_3O_4@SiO_2-NH-HCGs were investigated systematically for removal efficiency and conditions of Cu^{2+}, Hg^{2+}, Pb^{2+} and Cd^{2+}.

2 Experimental

2.1 Apparatus

Flame atomic adsorption spectrometric (FAAS) measurements were carried out on a Perkin Elmer Zeeman 1100 B spectrometer (Uberlingen, Germany) with an air/acetylene flame. Fourier transmission infrared spectra (FT-IR, 4000–300 cm^{-1}) in KBr were recorded on a Nicolet Nexus 470 FT-IR spectrometer (Nicolet, USA). Recorded on a micrographs of the adsorbents were obtained at 5.0 kV on a supra 40vp field emission scanning electron microscopy (FEI, Shanghai, USA). The morphology and particle size analysis were carried out on a transmission electron microscope (TEM) of H-7500 (Hitachi, Japan) with an acceleration voltage of 80 kV after dropping the nanoparticle sorbents suspended in ethanol onto copper grids. X-ray diffraction measurements (d8 Advance, Bruker, Germany) were taken to investigate the crystal structure of the Fe_3O_4@SiO_2-NH-HCGs. The pH measurements of all solutions were performed using a mettler toledo delta 320 pH meter (Mettler-Toledo Instruments Co. Ltd., Shanghai, China).

2.2 Materials

3-Aminopropyltriethoxysilane, 2-chloropyridine, 3-chloropyridazine, 2-chloropyrazine, 4-chloropyrimidine were purchased from J&K Scientific Ltd. (Beijing, China). $FeCl_3{\cdot}6H_2O$, $Cu(NO_3)_2$, $Cd(NO_3)_2$, $Hg(OAc)_2$, $Pb(OAc)_2$, ethylene glycol and polyethylene glycol 4000 were supplied by Sinopharm Chemical Reagent Co. Ltd. (Beijing, China). Concentrations of heavy metal solutions were controlled at 1.00 g l^{-1} in deionized water and were diluted subsequently to different concentration for next use.

2.3 Synthesis of magnetite nanoparticles (MNP)

MNP were synthesized by the method reported previously (30). Briefly, 1.35 g of $FeCl_3{\cdot}6H_2O$ and 3.60 g of sodium acetate were dissolved in 40 ml of ethylene glycol under to form a clear solution. Then 1 g of polyethylene glycol 4000 were added. The mixture was stirred until the reactants were fully dissolved. The resulting homogeneous yellow solution was transferred to a teflon-lined stainless steel autoclave, sealed, and heated at 180°C. The autoclave was cooled to room temperature after 12 h. The resulting black magnetite particles were washed several times with ethanol and dried in vacuum at 60°C for 6 h. Yield: 95.20%.

2.4 Synthesis of Fe_3O_4@SiO_2-NH_2

Fe_3O_4@SiO_2-NH_2 were prepared according to a previously reported method (31). Briefly, 0.20 g MNP were dispersed in 30.00 ml ethanol under ultrasonic for 15 min, then 0.80 ml APTES and 1 ml deionized water were added into the above dispersion at room temperature. The mixture was stirred vigorously for 6 h. The final products were collected by applying an external magnetic field, washed with ethanol and then dried under vacuum at 60°C for 6 h. Yield: 86.80%.

2.5 Synthesis of Fe_3O_4@SiO_2-NH-HCGs

Fe_3O_4@SiO_2-NH-HCGs were synthesized by substitution reaction of Fe_3O_4@SiO_2-NH_2 and 2-chloropyridine, 3-chloropyridazine, 2-chloropyrazine, 4-chloropyrimidine, respectively. Briefly, 0.20 g Fe_3O_4@SiO_2-NH-HCGs were dispersed in 30.00 ml 2-propanol under mechanical agitation for 30 min, then 0.21 ml 2-chloropyridine was added into the above solution at room temperature, continued stirring for 6 h. Fe_3O_4@SiO_2-NH-py was collected by applying an external magnetic field, washed with ethanol and then dried under vacuum at 60°C for 6 h (yield: 98.10%). Subsequently, Fe_3O_4@SiO_2-NH-pyd was obtained in the same way as for Fe_3O_4@SiO_2-NH-py by using 0.20 ml 3-chloropyridazine instead of 0.21 ml 2-chloropyridine (yield: 97.50%), Fe_3O_4@SiO_2-NH-pya was obtained in the same way as for Fe_3O_4@SiO_2-NH-py by using 0.20 ml 2-chloropyrazine instead of 0.21 ml 2-chloropyridine (yield: 96.70%), Fe_3O_4@SiO_2-NH-pym was obtained in the same way as for Fe_3O_4@SiO_2-NH-py by using 0.26 g 4-chloropyrimidine instead of 0.21 ml 2-chloropyridine (yield: 96.30%).

2.6 Batch procedure

First, standard 0.10 M hydrochloric acid and 0.10 M sodium hydroxide solutions were used for pH adjustment. The effect of pH on the static removal efficiency of Cu^{2+}, Hg^{2+}, Pb^{2+} and Cd^{2+} were examined, respectively by equilibrating 0.10 g of Fe_3O_4@SiO_2-NH-HCGs with 50.00 ml of sample solutions containing 10.00 mg l^{-1} of single target metal ion under different pH conditions.

Second, contacting time of Cu^{2+}, Hg^{2+}, Pb^{2+} and Cd^{2+} onto the Fe_3O_4@SiO_2-NH-HCGs were also examined, respectively by equilibrating 0.10 g of Fe_3O_4@SiO_2-NH-HCGs with 50.00 ml of sample solutions containing 10.00 mg l^{-1} of single target metal ion at pH=7.0.

Third, maximum adsorption capacity was measured, respectively by equilibrating 0.10 g of Fe_3O_4@SiO_2-NH-HCGs with 50.00 ml of various concentrations of single target metal ion solutions at pH=7.0. In order to reach the "saturation", single target metal ion concentration was increased till the plateau values (adsorption capacity values) was obtained.

In the above batch experiments, the mixtures were dispersed by ultrasonic for 10 min at room temperature. After adsorption reached equilibrium, Fe_3O_4@SiO_2-NH-HCGs were conveniently separated via an external magnetic field and the solution was collected for metal ions concentration measurements. Fe_3O_4@SiO_2-NH-HCGs were washed thoroughly with deionized water to neutrality. The concentrations of metal ions were determined by FAAS. In order to obtain reproducible experimental results, the adsorption experiments were carried out at least three times.

The adsorption capacity, removal efficiency were calculated as the following equations:

$$Q=(C_o\text{-}C_e)V/W,\ E=(C_o\text{-}C_e)/C_o$$

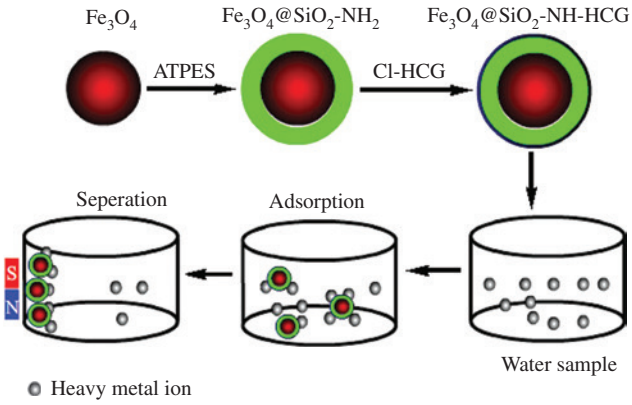

Scheme 1: Synthesis route of Fe_3O_4@SiO_2-NH-HCG nanoparticles and their application for removal of heavy metal ions with the help of an external magnetic field.

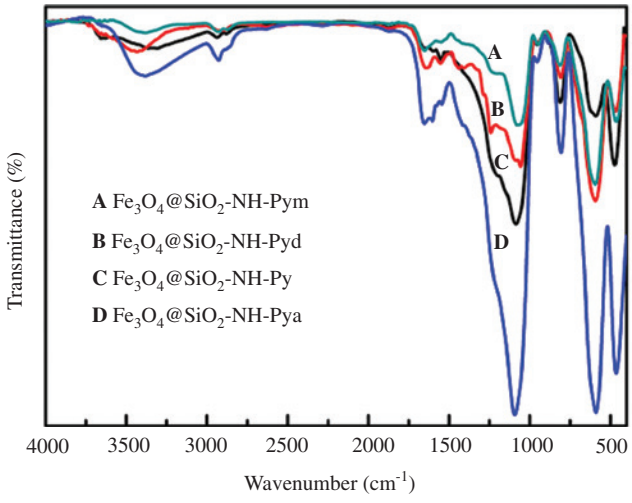

Figure 1: The FT-IR spectra of Fe_3O_4@SiO_2-NH-HCGs.

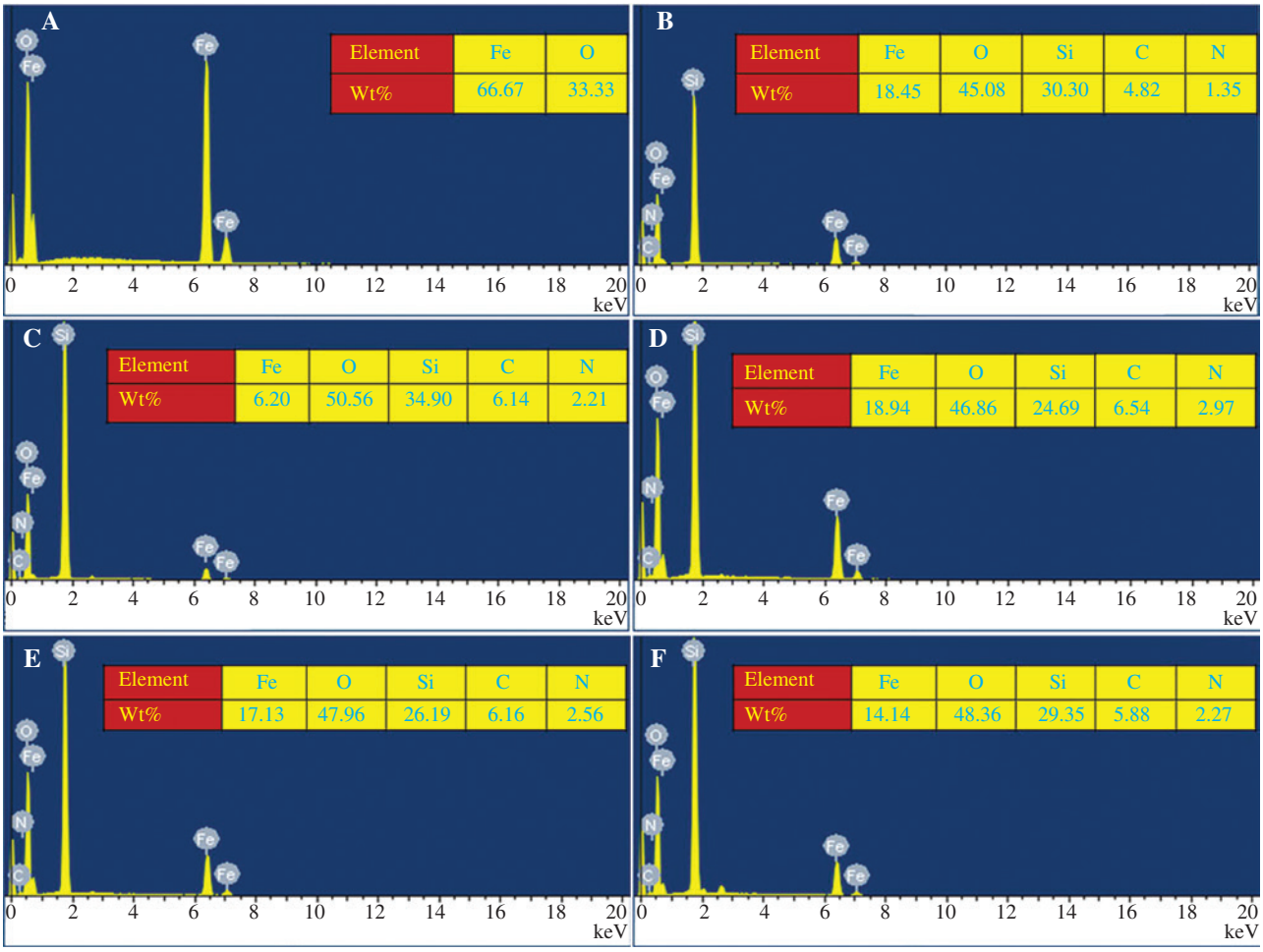

Figure 2: EDS spectra of Fe_3O_4 (A), Fe_3O_4@SiO_2-NH_2 (B) and Fe_3O_4@SiO_2-NH-HCGs (HCG=C: Py; D: Pyd; E: Pya; F: Pym).

where Q represents the adsorption capacity (mg g^{-1}), E is removal efficiency (%), C_o and C_e are the initial and equilibrium concentration of heavy metal ions (mg l^{-1}), W is the mass of Fe_3O_4@SiO_2-NH-HCG (g) and V is the volume of heavy metal ion solution (L).

The reactions during the experiment are also illustrated in detail in Scheme 1.

3 Results and discussion

3.1 Characterization studies

The FT-IR spectra of Fe_3O_4@SiO_2-NH-HCGs are shown in Figure 1, the strong band at 1096 cm^{-1} is due to the stretching bonds of Si-O-Si (32). The band at 812 cm^{-1} is assigned to the Si-O-Si symmetric stretch, while the sharp band at 471 cm^{-1} corresponds to the Si-O-Si or O-Si-O bending mode. The band at 590 cm^{-1} is an indication of the presence of Si-O-Fe (33). The bands at 3500 and 2950 cm^{-1} are presence of N-H and -CH_2-. The bands at 1650 and 1480 cm^{-1} are attributed to vibrations in the aromatic ring and the

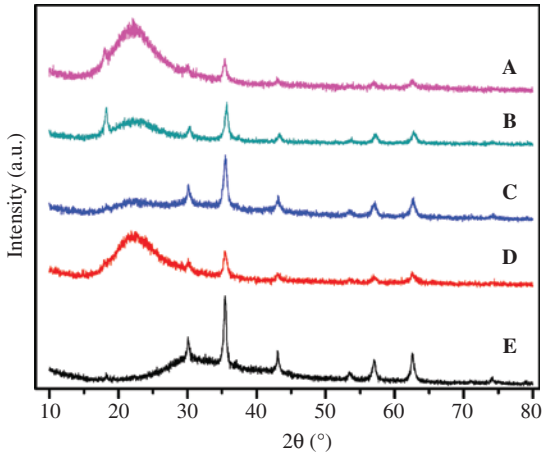

Figure 3: XRD pattern of Fe_3O_4 (E) and Fe_3O_4@SiO_2-NH-HCGs (HCG=A: Py; B: Pyd; C: Pya; D: Pym).

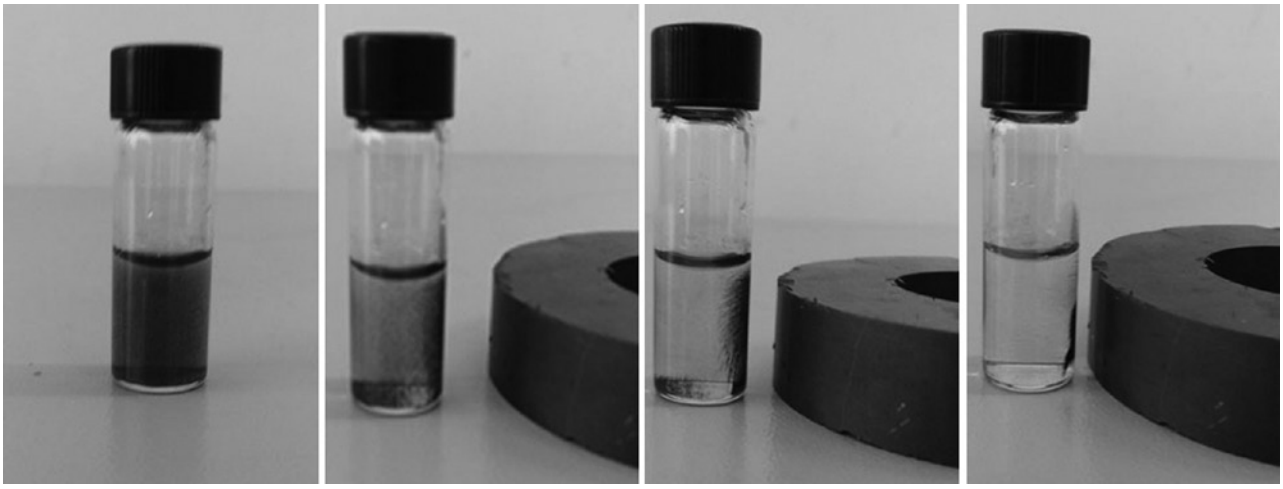

Figure 4: Separation process of Fe_3O_4@SiO_2-NH-HCGs under an external magnetic field.

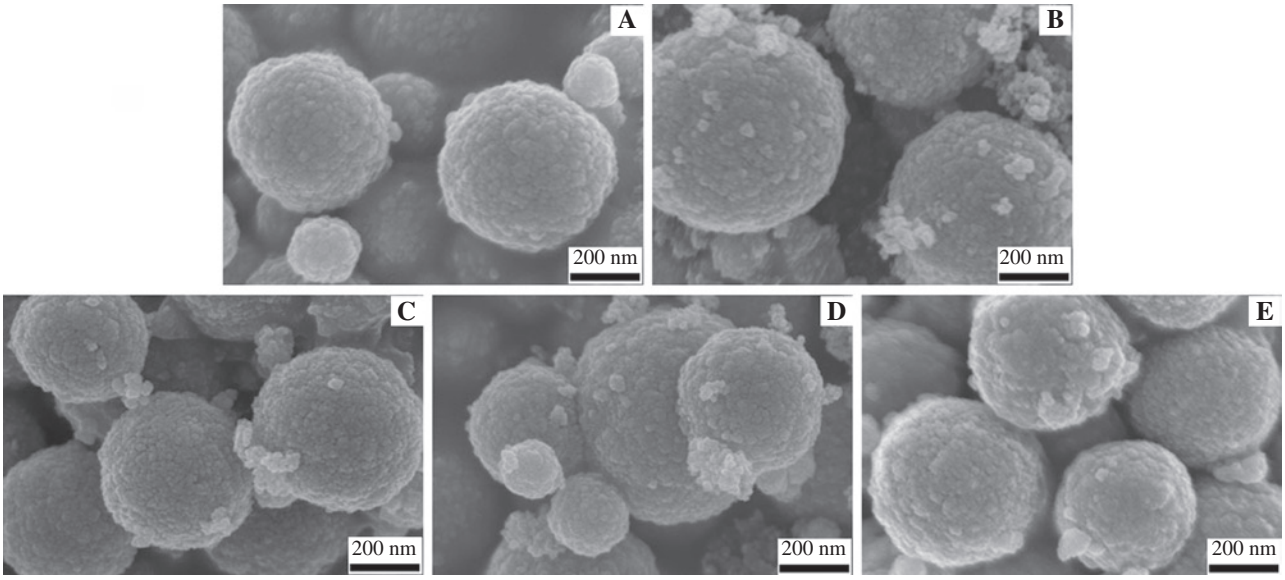

Figure 5: SEM images of Fe_3O_4 (A) and Fe_3O_4@SiO_2-NH-HCGs (HCG=B: Py; C: Pyd; D: Pya; E: Pym).

C-N stretching modes (27), respectively. The appearance of these adsorption peaks indicates that Fe_3O_4@SiO_2-NH-HCGs have been synthesized successfully (34). The shapes of Fe_3O_4@SiO_2-NH-HCGs are similar due to the similar structure.

The EDS spectrum of prepared composites is shown in Figure 2. The EDS spectrum of Fe_3O_4 shows the peaks originated from iron and oxygen elements (Figure 2A). With the presence of nitrogen and other elements, the peak intensity of iron element reduces evidently in Figure 2B–F. The content of nitrogen element in Fe_3O_4@SiO_2-NH-HCGs is higher than that of Fe_3O_4@SiO_2-NH_2, which is due to contribution of *N*-heterocyclic groups. These results indicate that the successful surface covering of Fe_3O_4 nanoparticles with APTES and successful grafting of *N*-heterocyclic groups on the surface of composite materials.

X-ray powder diffraction (XRD) patterns of pure Fe_3O_4 and Fe_3O_4@SiO_2-NH-HCGs are shown in Figure 3, indicating the existence of iron oxide particles (Fe_3O_4), which has superparamagnetic properties and can be used for the magnetic separation. The XRD analysis results of pure Fe_3O_4 and Fe_3O_4@SiO_2-NH-HCGs were mostly coincident. Six characteristic peaks of Fe_3O_4 (2θ=30.1°, 35.5°, 43.3°, 53.4°, 57.2° and 62.5°) were observed in the XRD pattern. These are related to the (220), (311), (400), (422), (511) and (440) planes of Fe_3O_4 spinel structure (35).

We select one of Fe_3O_4@SiO_2-NH-HCGs to demomstrate separation process under an external magnetic field

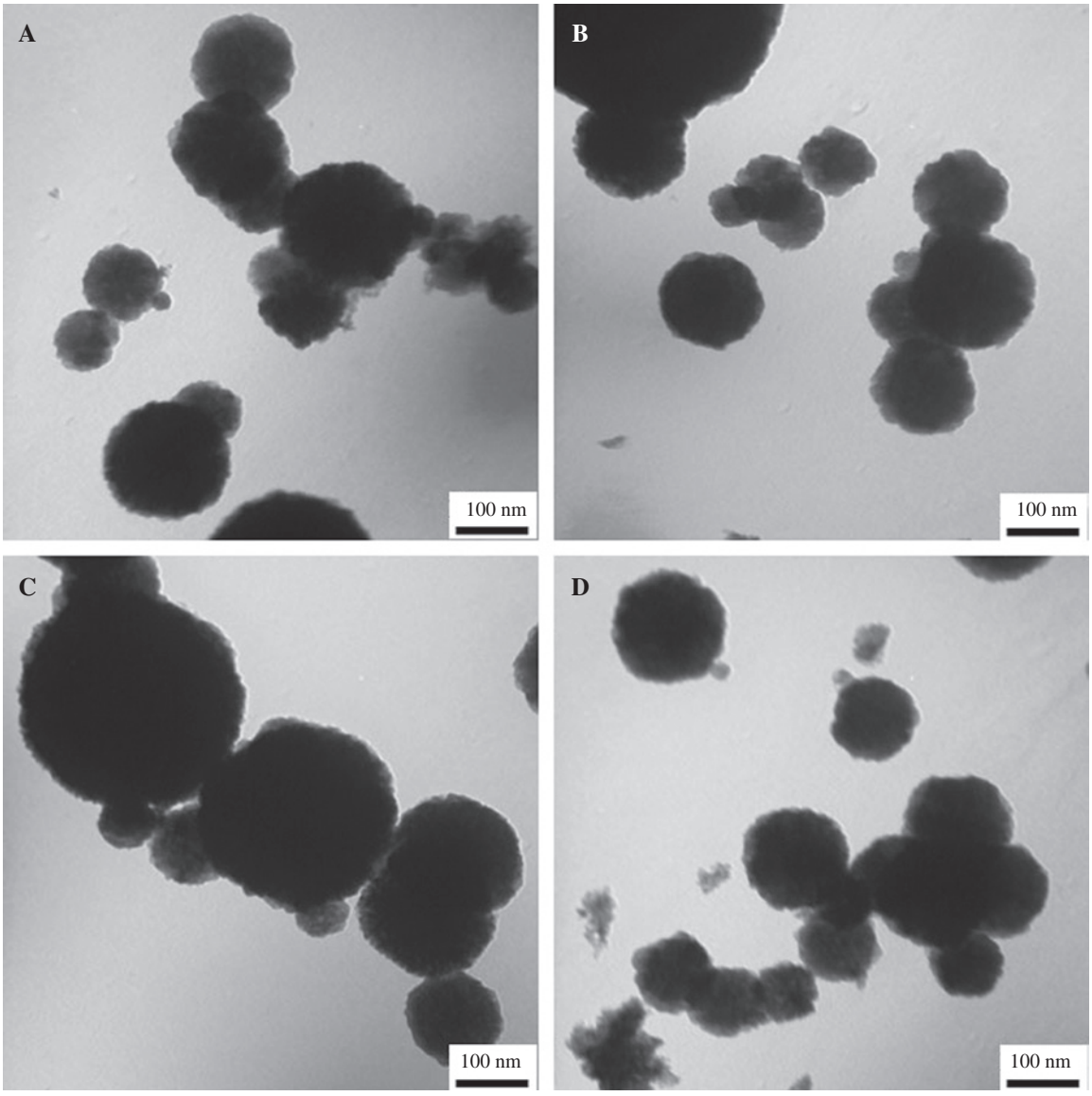

Figure 6: TEM images of Fe_3O_4@SiO_2-NH-HCGs (HCG=A: Py; B: Pyd; C: Pya; D: Pym).

after adsorb heavy metal ions in water solution. As shown in Figure 4, the black magnetic particles in homogeneous solution start moving towards the magnet under an external magnet, the moving process of the black magnetic particles are well demonstrated in second and third photographs. At last, the black particles are separated successfully from the solution, indicating the black particles have excellent superparamagnetic properties.

As shown in Figure 5, from the sem images with same resolutions, Fe_3O_4@SiO_2-NH-HCGs have similar morphologies, exhibiting more roughness than that of free Fe_3O_4 (A). It can be clearly observed that many modified silicas are located on the Fe_3O_4 nanoparticles' surfaces.

TEM are used to investigate the internal morphology of Fe_3O_4@SiO_2-NH-HCGs. As shown in Figure 6, the dark magnetic particles are individually coated with gray silica shell. This further confirms that Fe_3O_4@SiO_2-NH-HCGs have been prepared successfully.

3.2 Effect of pH

The pH condition has been considered as playing a key role in adsorb investigations because it often affects the amounts of adsorbed metals. Figure 7 shows, respectively, the removal (%) of heavy metal ions onto every Fe_3O_4@SiO_2-NH-HCGs as a function of variable pH. The change trend of the heavy metal ions removal efficiency onto every Fe_3O_4@SiO_2-NH-HCGs are similar with the

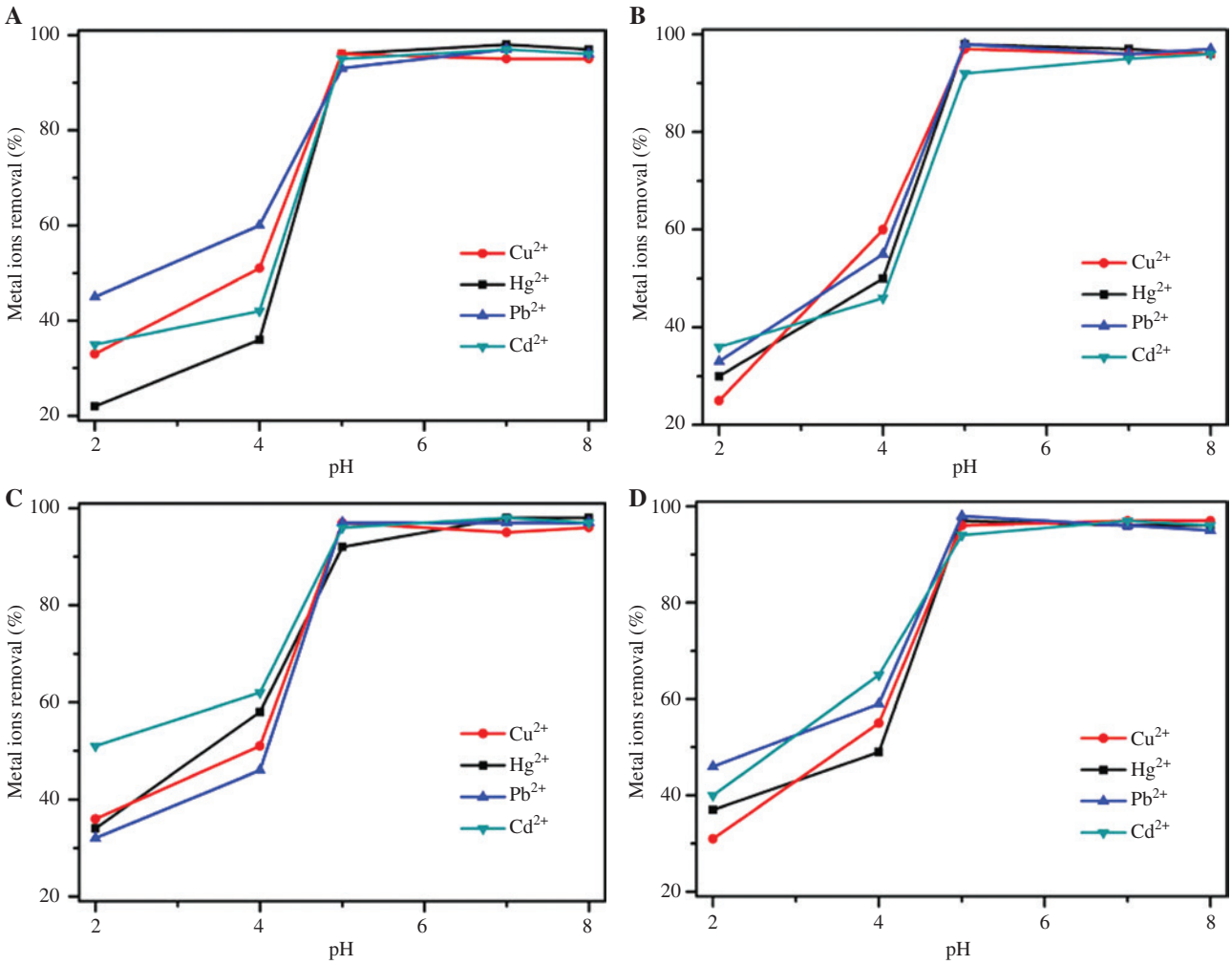

Figure 7: The effect of pH on the removal efficiency of toxic ions using Fe_3O_4@SiO_2-NH-HCGs (HCG=A: Py; B: Pyd; C: Pya; D: Pym).

increase of pH value due to similar structural magnetic adsorbents. The removal efficiency is lower owing to the protonation of Fe_3O_4@SiO_2-NH-HCGs, diminishing donor nitrogen atoms below pH 5.0. The most ideal pH range in 5.0~8.0, the removal efficiency is generally above 96%. In the higher pH ranges, These heavy metal ions get out of the solution due to formation of hydroxide (36). These formation of insoluble metal hydroxide species instead of free heavy metal ions also decreased their adsorption efficiency. Therefore, no adsorption experiment were performed at higher pH.

3.3 Effect of contacting time on the removal efficiency

In order to determine the effect of contacting time on metal extraction, further experiments were carried out at room temperature and pH 7.0 with the contacting time varying in the range of 30 min. Figure 8 shows the effect of contacting time on the removal efficiency of Cu^{2+}, Hg^{2+}, Pb^{2+} and Cd^{2+} using different Fe_3O_4@SiO_2-NH-HCGs. At first, the removal efficiency of toxic ions improve constantly with the increase of contacting time due to prolonged time may promote the access of ions to active sites on the surface of adsorbent. With the disappearance gradually of the active site, the time point of equilibrium appears. No matter what kind of toxic ions is removed by Fe_3O_4@SiO_2-NH-HCGs, it is clear that the removal efficiency is generally above 96% just 20 min. The results show that the removal efficiency of Fe_3O_4@SiO_2-NH-HCGs is high efficiency.

3.4 Maximum adsorption capacity

Adsorption of toxic ions from aqueous solution were investigated in batch experiments with stirring for 1 h.

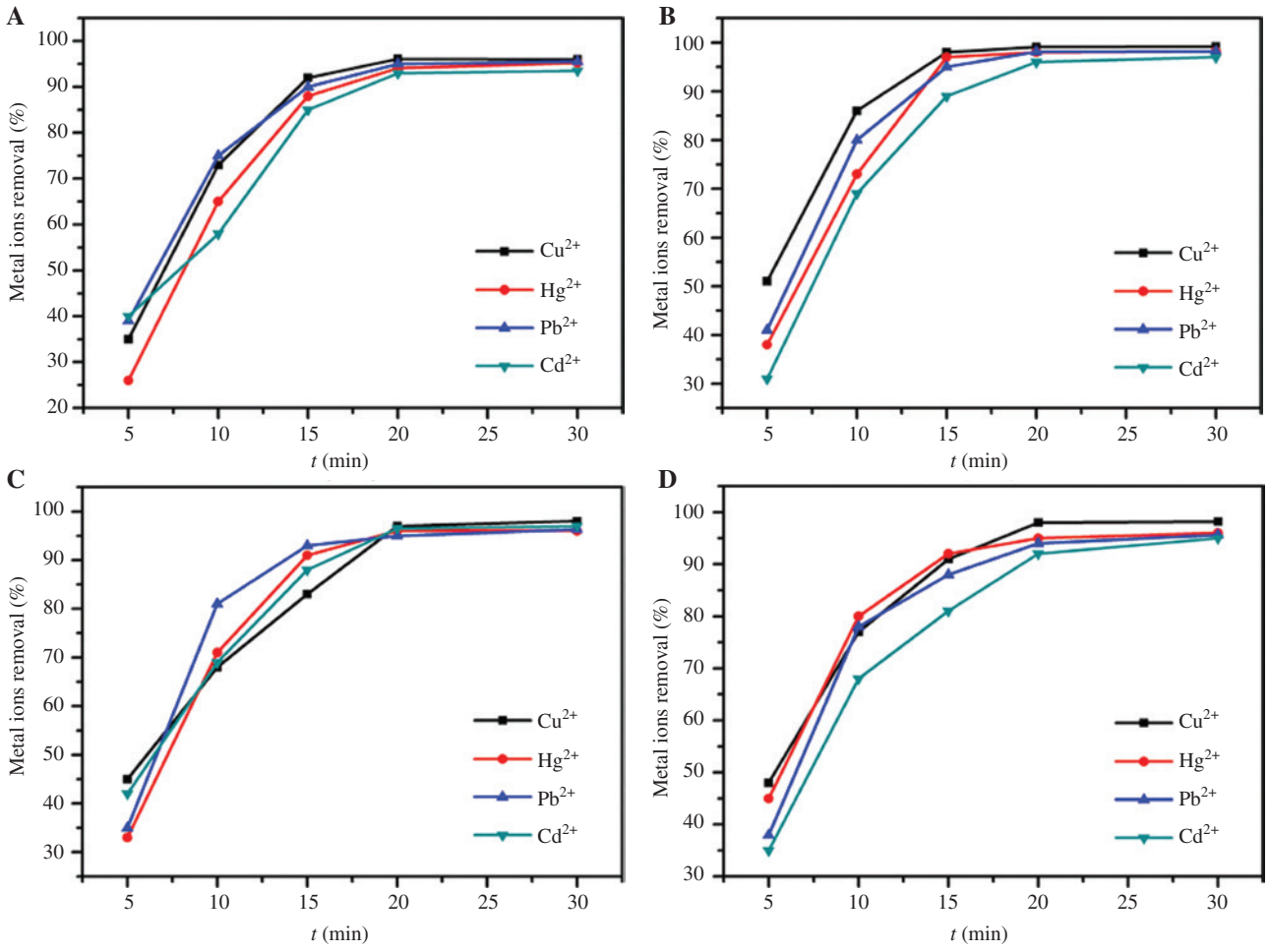

Figure 8: The effect of contacting time on the removal efficiency of toxic ions using Fe_3O_4@SiO_2-NH-HCGs (HCG=A: Py; B: Pyd; C: Pya; D: Pym).

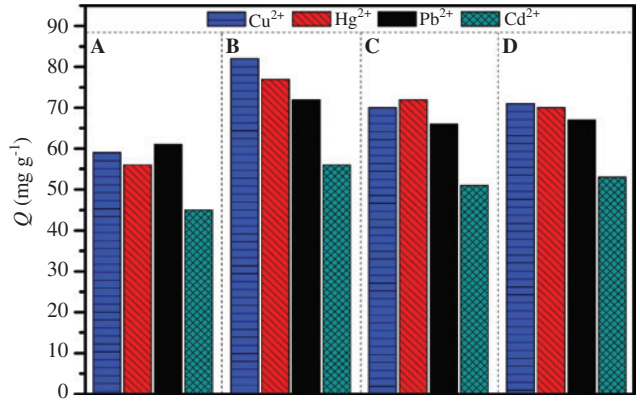

Figure 9: Maximum adsorption capacity of Fe_3O_4@SiO_2-NH-HCGs (HCG=A: Py; B: Pyd; C: Pya; D: Pym).

As can be seen in Figure 9, as for the sample of Fe_3O_4@SiO_2-NH-py (Figure 9A), the maximum adsorption capacity (Q_{max}) of Cu^{2+}, Hg^{2+}, Pb^{2+} and Cd^{2+} are 59, 56, 61, and 45 mg g^{-1}, respectively. The Q_{max} of single target metal ion is the lowest among four adsorbents due to containing the lowest nitrogen atom proportion compared with other adsorbents. However, the Q_{max} of Cu^{2+}, Hg^{2+}, Pb^{2+} and Cd^{2+} by Fe_3O_4@SiO_2-NH-pyd are 82, 77, 72, and 56 mg g^{-1}, respectively (Figure 9B). The Q_{max} of single target metal ion is the highest due to the two nitrogen atoms located in the same side of the aromatic ring, being beneficial to coordination with heavy metal ions. Figure 9C and D show the Q_{max} of Cu^{2+}, Hg^{2+}, Pb^{2+} and Cd^{2+} by Fe_3O_4@SiO_2-NH-pya and Fe_3O_4@SiO_2-NH-pym, respectively. For the same target metal ion, their Q_{max} are almost the same due to similar coordination mode. Additionally, for the same adsorbent, the Q_{max} of Cd^{2+} is the lowest while the Q_{max} of Cu^{2+} is generally the highest, probably due to different coordination ability of metal ions and nitrogen atom. The Q_{max} of Hg^{2+} in Fe_3O_4@SiO_2-NH-HCGs is higher than that of reported Fe_3O_4-R6G material (27), which is due to the high nitrogen atom proportion and low steric hindrance of grafting group.

Table 1: Eleven cycles of adsorption-desorption of different metal ions onto the Fe_3O_4@SiO_2-NH-HCG.

Adsorbents	Metal ions	Removal efficiency of cycles (%)										
		1	2	3	4	5	6	7	8	9	10	11
Fe_3O_4@SiO_2-NH-Py	Cu^{2+}	100	99	96	95	94	93	93	85	82	76	68
	Hg^{2+}	100	99	98	97	96	96	95	93	89	85	80
	Pb^{2+}	100	99	99	98	97	95	95	94	94	92	85
	Cd^{2+}	100	99	98	98	97	96	96	95	95	92	76
Fe_3O_4@SiO_2-NH-Pyd	Cu^{2+}	100	99	99	98	98	98	96	94	93	86	82
	Hg^{2+}	100	99	98	98	96	96	95	93	89	82	74
	Pb^{2+}	100	98	97	97	96	95	95	92	90	85	80
	Cd^{2+}	100	98	96	95	95	94	93	90	89	85	81
Fe_3O_4@SiO_2-NH-Pya	Cu^{2+}	100	98	98	97	96	96	95	94	92	90	87
	Hg^{2+}	100	99	99	98	97	97	96	96	93	92	90
	Pb^{2+}	100	99	98	97	96	96	95	95	93	82	76
	Cd^{2+}	100	98	97	97	97	95	95	93	89	82	73
Fe_3O_4@SiO_2-NH-Pym	Cu^{2+}	100	99	98	97	97	96	95	95	90	85	80
	Hg^{2+}	100	99	98	98	96	95	95	94	90	88	86
	Pb^{2+}	100	98	97	96	95	94	92	88	83	72	67
	Cd^{2+}	100	99	97	97	96	95	95	93	92	90	83

4 Selection of eluents

Desorption studies were carried out using acetic acid (0.20 M, 0.50 M and 1.00 M), hydrochloric acid (0.20 M, 0.50 M and 1.00 M) and nitric acid (0.20 M, 0.50 M and 1.00 M) as eluents and all the regeneration experiments were carried out at room temperature. Experimental results showed that 0.50 M hydrochloric acid had 95% desorption efficiency for Fe_3O_4@SiO_2-NH-HCG containing heavy metal ions. Thus, 0.50 M hydrochloric acid was selected as optimal eluent.

4.1 Reusability

In order to study the reusing possibility of Fe_3O_4@SiO_2-NH-HCGs, they were subjected to several loading and elution operations. The loading operations were carried out by saturating 0.10 g of Fe_3O_4@SiO_2-NH-HCG in 100.00 ml 1.00 g l^{-1} single target metal ion solution. The elution operations were carried out by shaking Fe_3O_4@SiO_2-NH-HCG which contained maximum amount of metal ion in 100.00 ml 0.50 mol l^{-1} hydrochloric acid. The removal efficiency were calculated from the loading and elution tests. The results of eleven cycles of adsorption-desorption of different metal ions onto the Fe_3O_4@SiO_2-NH-HCG are shown in Table 1. The dynamic removal efficiency of different metal ions were not significantly decreased even after seven cycles. These results indicate that the Fe_3O_4@SiO_2-NH-HCGs possess excellent stability and reusability.

5 Conclusion

In summary, four kinds of novel Fe_3O_4@SiO_2-NH-HCGs were successfully formed by grafting of different heterocyclic groups on Fe_3O_4@SiO_2-NH_2 via substitution reaction. The grafting method is simple and efficient, and the yield of all products are over 96%. Batch experiments were performed to evaluate adsorption conditions of Cu^{2+}, Hg^{2+}, Pb^{2+} and Cd^{2+}. Under the normal temperature and neutral condition, just 20 min, the removal efficiency of any Fe_3O_4@SiO_2-NH-HCGs is more than 96%. The results show that the removal efficiency of Fe_3O_4@SiO_2-NH-HCGs is high efficiency. As far as Q_{max} of Fe_3O_4@SiO_2-NH-HCGs are concerned, Q_{max} of different kinds of adsorbents is different. Q_{max} of Fe_3O_4@SiO_2-NH-pyd is the highest due to the two nitrogen atoms located in the same side of the aromatic ring, being beneficial to coordination with heavy metal ions. These Fe_3O_4@SiO_2-NH-HCGs have good stability and reusability, their removal efficiency have no obvious decrease after being used seven times. After the experiments were finished, Fe_3O_4@SiO_2-NH-HCGs were conveniently separated via an external magnetic field due to superparamagnetism. These results indicate that these Fe_3O_4@SiO_2-NH-HCGs are potentially attractive materials for the removal of heavy metal ions from industrial wastewater.

Acknowledgments: This work was supported by the National Natural Science Foundation of China (No. 21164011) and Xinjiang Key Laboratory of Plant Resources & Natural Products Chemistry.

References

1. Kwon JS, Yun ST, Lee JH, Kim SH, Jo HY. Removal of divalent heavy metals (Cd, Cu, Pb, and Zn) and arsenic(III) from aqueous solutions using scoria: kinetics and equilibria of sorption. J Hazard Mater. 2010;174:307–13.
2. Hultberg B, Andersson A, Isaksson A. Alterations of thiol metabolism in human cell lines induced by low amounts of copper, mercury or cadmium ions. Toxicology. 1998;126:203–12.
3. Antochshuk V, Jaroniec M. 1-Allyl-3-propylthiourea modified mesoporous silica for mercury removal. Chem Commun. 2002;258–9.
4. Rozada F, Otero M, Morán A, García AI. Adsorption of heavy metals onto sewage sludge-derived materials. Bioresour Technol. 2008;99:6332–8.
5. Memon S, Yilmaz M. An excellent approach towards the designing of a schiff-base type oligocalix [4] arene, selective for the toxic metal ions. J Macromol Sci Part A-Pure Appl Chem. 2002;39:63–73.
6. Raut DR, Mohapatra PK, Ansari SA, Sakar A, Manchanda VK. Selective transport of radio-cesium by supported liquid membranes containing calix[4]crown-6 ligands as the mobile carrier. Desalination. 2008;232:262–71.
7. Fu F, Wang Q. Removal of heavy metal ions from wastewaters: a review. J Environ Manage. 2011;92:407–18.
8. Jha MK, Kumar V, Maharaj L, Singh R. Studies on Leaching and Recycling of Zinc from Rayon Waste Sludge. J Ind Eng Chem Res. 2004;43:1284–95.
9. Kentish SE, Stevens GW. Innovations in separations technology for the recycling and re-use of liquid waste streams. Chem Eng J. 2001;84:149–59.
10. Jha MK, Upadhyay RR, Lee JC, Kumar V. Treatment of rayon waste effluent for the removal of Zn and Ca using indion BSR resin. Desalination. 2008;228:97–107.
11. Zhang SX, Zhang YY, Liu JS, Xu Q, Xiao HQ, Wang XY, Xu H, Zhou J. Thiol modified Fe_3O_4@SiO_2 as a robust, high effective, and recycling magnetic sorbent for mercury removal. Chem Eng J. 2013;226:30–8.
12. Xie L, Jiang R, Zhu F, Liu H, Ouyang G. Application of functionalized magnetic nanoparticles in sample preparation. Anal Bioanal Chem. 2014;406:377–99.
13. Monier M, Abdel-Latif DA. Synthesis and characterization of ion-imprinted chelating fibers based on PET for selective removal of Hg^{2+}. Chem Eng J. 2013;221:452–60.
14. Chen CL, Hu J, Shao DD, Li JX, Wang XK. Adsorption behavior of multiwall carbon nanotube/iron oxide magnetic composites for Ni(II) and Sr(II). J Hazard Mater. 2009;164:923–8.
15. Zhang Y, Yan L, Xu W, Guo X, Cui L, Gao L, Wei Q, Du B. Adsorption of Pb(II) and Hg(II) from aqueous solution using magnetic $CoFe_2O_4$-reduced graphene oxide. J Mol Liq. 2014;191:177–82.
16. Hu HB, Wang ZH, Pan L. Synthesis of monodisperse Fe_3O_4@silica core–shell microspheres and their application for removal of heavy metal ions from water. J Alloy Compd. 2010;492:656–61.
17. Sun SH, Zeng H. Size-controlled synthesis of magnetite nanoparticles. J Am Chem Soc. 2002;124:8204–5.
18. Lu AH, Salabas EL, Schüth F. Magnetic nanoparticles: synthesis, protection, functionalization, and application. Angew Chem Int Ed. 2007;46:1222–44.
19. Jing Y, Moore LR, Williams PS, Chalmers JJ, Farag SS, Bolwell B, Zborowski M. Blood progenitor cell separation from clinical leukapheresis product by magnetic nanoparticle binding and magnetophoresis. Biotech Bioeng. 2007;96:1139–54.
20. Lee JH, Jun YW, Yeon SI, Shin JS. Dual-mode nanoparticle probes for high-performance magnetic resonance and fluorescence imaging of neuroblastoma. Angew Chem Int Ed. 2006;45:8160–2.
21. Neuberger T, Schopf B, Hofmann H, Hofmann M, von Rechenberg B. Superparamagnetic nanoparticles for biomedical applications: possibilities and limitations of a new drug delivery system. J Magn Magn Mater. 2005;293:483–96.
22. Gu H, Xu K, Xu C, Xu B. Biofunctional magnetic nanoparticles for protein separation and pathogen detection. Chem Commun (Camb). 2006;9:941–9.
23. Takafuji M, Ide S, Ihara H, Xu Z. Preparation of poly(1-vinylimidazole)-grafted magnetic nanoparticles and their application for removal of metal ions. Chem Mater. 2004;16:1977–83.
24. Wu Z, Wu J, Xiang H, Chun MS, Lee K. Organosilane-functionalized Fe_3O_4 composite particles as effective magnetic assisted adsorbents. Colloid Surf A. 2006;279:167–74.
25. Wu W, He Q, Jiang C. Magnetic iron oxide nanoparticles: synthesis and surface functionalization strategies. Nanoscale Res Lett. 2008;3:397–415.
26. Zhang SX, Zhang YY, Liu JS, Xu Q, Xiao HQ, Wang XY, Xu H, Zhou J. Thiol modified Fe_3O_4@SiO_2 as a robust, high effective, and recycling magnetic sorbent for mercury removal. Chem Eng J. 2013;226:30–8.
27. Wang ZQ, Wu DY, Wu GH, Yang NN, Wu AG. Modifying Fe_3O_4 microspheres with rhodamine hydrazide for selective detection and removal of Hg^{2+} ion in water. J Hazard Mater. 2013;244–245:621–7.
28. Wang YY, Li B, Zhang LM, Li P, Wang LL, Zhang J. Multifunctional magnetic mesoporous silica nanocomposites with improved sensing performance and effective removal ability toward Hg(II). Langmuir. 2012;28:1657–62.
29. Mahdaviana AR, Mirrahimib MAS. Efficient separation of heavy metal cations by anchoring polyacrylic acid on superparamagnetic magnetite nanoparticles through surface modification. Chem Eng J. 2010;59:264–71.
30. Shao MF, Ning FY, Zhao JW, Wei M, Evans DG, Duan X. Preparation of Fe_3O_4@SiO_2@layered double hydroxide core-shell microspheres for magnetic separation of proteins. J Am Chem Soc. 2012;134:1071–7.
31. Khoee S, Abedini N. One-pot synthesis of amphiphilic nanogels from vinylated SPIONs/HEMA/PEG via a combination of click chemistry and surfactant-free emulsion photopolymerization: unveiling of the protein-nanoparticle interactions. Polymer. 2014;55:5635–47.
32. Du GH, Liu ZL, Xia X, Chu Q, Zhang SM. Characterization and application of Fe_3O_4/SiO_2 nanocomposites. J Sol-Gel Sci Techn. 2006;39:285–91.
33. Figueira P, Lopes CB, Daniel-da-Silva AL, Pereira E, Duarte AC, Trindade T. Removal of mercury (II) by dithiocarbamate surface functionalized magnetite particles: application to synthetic and natural spiked waters. Water Res. 2011;45:5773–84.
34. Wang XN, Liang RP, Meng XY, Qiu JD. One-step synthesis of mussel-inspired molecularly imprinted magnetic polymer as stationary phase for chip-based open tubular capillary electrochromatography enantioseparation. J Chromatogr A. 2014;1362:301–8.
35. Xuan SH, Xiang Y, Wang J, Leung KCF, Shu KY. Synthesis of Fe_3O_4@ polyaniline core/shell microspheres with well-defined blackberry-like morphology. J Phys Chem C. 2008;112:18804–9.
36. Shen XF, Wang Q, Chen WL, Pang YH. One-step synthesis of water-dispersible cysteine functionalized magnetic Fe_3O_4 nanoparticles for mercury(II) removal from aqueous solutions. Appl Surf Sci. 2014;317:1028–34.